3rd China-Japan Joint Workshop on Positron Science (JWPS2017)
JJAP Conf. Proc. **7**, 011105 (2018) https://doi.org/10.7567/JJAPCP.7.011105

Effect of Helium Irradiation Fluence on He_nV_m Cluster Evolution in Nickel Studied by Positron Annihilation Spectroscopy

Yihao Gong[1,2], Shuoxue Jin[1], Eryang Lu[1], Te Zhu[1,2], Ligang Song[1,2], Daqing Yuan[3], Baoyi Wang[1,2], and Xingzhong Cao[1*]

[1] *Institute of High Energy Physics, Chinese Academy of Sciences, Beijing, 100049, China*
[2] *University of Chinese Academy of Sciences, Beijing, 100039, China*
[3] *China Institute of Atomic Energy, Beijing, 102413, China*

E-mail: caoxzh@ihep.ac.cn

(Received October 30, 2017)

Polycrystalline nickel was irradiated using 50 keV He ions at room temperature. The irradiated fluences were 5×10^{13} He^+ cm^{-2}, 5×10^{14} He^+ cm^{-2}, and 5×10^{15} He^+ cm^{-2}, respectively. Positron annihilation Doppler broadening spectroscopy (DBS) was used to characterize the irradiation-induced defect evolution. The DBS results show that a large amount of vacancy defects were introduced in the specimens after helium irradiation. In addition, the DBS data could be also interpreted as the formation of helium-vacancy (He_nV_m) clusters due to combination between vacancies and helium atoms.

1. Introduction

Nickel based alloys are potential structural materials in thorium molten salt reactors (TMSR) and supercritical water reactors (SCWR), due to their high molten salt corrosion resistance, creep resistance and high temperature strength [1–4]. The working circumstance of such structural materials is extreme, including high energy and flux neutron irradiation at high pressure and temperature. It is well known that interstitials and vacancies are produced by neutron displacement cascade [5]. Meanwhile, helium atoms are easily generated by (n, α) nuclear reactions [6]. The combination of vacancies and helium atoms forms He_nV_m clusters which are the primal nucleation sites of helium bubbles in structural materials. The existence of helium bubbles can enhance void swelling, surface blistering and degradation of mechanical properties [7–9]. Therefore, it is very important to investigate He_nV_m cluster evolution in nickel based alloys. Nickel based alloys are complicated and it is difficult to investigate the effect of helium irradiation fluence in these structural materials. Therefore nickel, as a typical face centered cubic material, was used in order to avoid interference from other components in the alloys. In the present work, positron annihilation Doppler broadening spectroscopy (DBS) was used to investigate the evolution of irradiation-induced defects since positrons are easily trapped by open space type defects [10].

2. Experimental detail

Polycrystalline nickel (purity: 99.999 %) was used and the specimens were cut to $10 \times 10 \times 0.3$ mm^3 in size. The surface of each specimen was polished to a mirror-like finish through a combination of mechanical polishing and electrochemical polishing. All specimens were then annealed at 1223 K for 2 h at high vacuum ($\sim 10^{-5}$ Pa). In the present work, helium ion irradiation was performed at the HI-13 tandem accelerator facility at the China Institute of Atomic Energy (CIAE). Irradiation was carried out using 50 keV helium ions at room temperature, and irradiation fluences were 5×10^{13} He^+ cm^{-2},

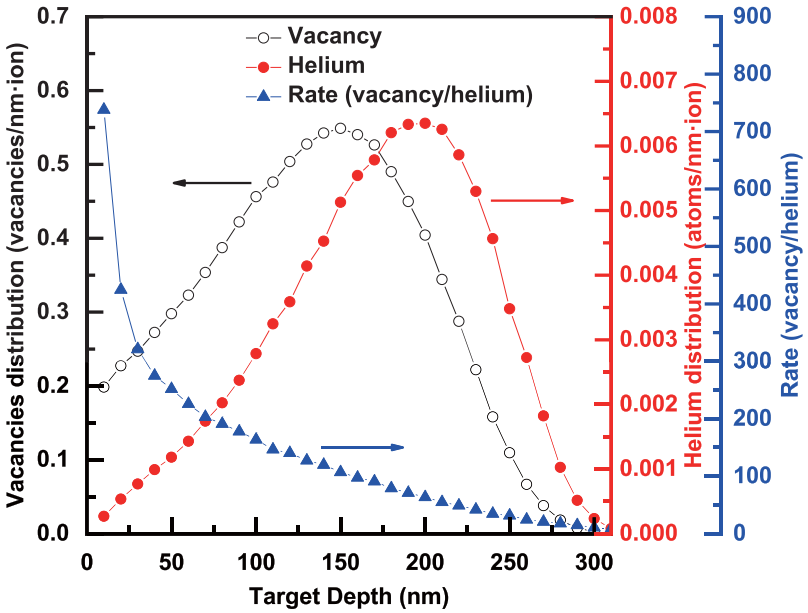

Fig. 1 Depth distribution of vacancies and helium atoms in 50 keV helium ion irradiated nickel calculated by SRIM2013.

5×10^{14} He^+ cm^{-2} and 5×10^{15} He^+ cm^{-2}. The stopping and range of ions in matter (SRIM) software code was used to calculate the helium atom and vacancy distribution in nickel, and the results are shown in Fig. 1. The displacement energy of nickel was set to 40 eV in the SRIM simulation [11].

Mono-energetic positrons were implanted into the specimens with the implantation energy varied from 0.1 keV to 20 keV. Positrons are generated by a 0.713 GBq ^{22}Na radiation source and moderated by a solid Ne moderator. A high-purity germanium detector (HPGe) was used to detect one of the annihilation γ-rays from the positron annihilation. The positron momentum is around 0.025 eV after thermalization so that the energy of the γ-ray photon mostly conveys information on the electron momentum [12]. The shape of the 511 keV γ-ray peak can then be parameterized with parameters which characterize the momentum distribution of annihilated electron. The S parameter is defined as the ratio of counts in the low-momentum region (zero to 3.0×10^{-3} m_0c, where m_0 is the electron rest mass and c is the speed of light) and the W parameter as the ratio of counts in high-momentum region (10.0×10^{-3} m_0c–23.0×10^{-3} m_0c) to the total counts in the annihilation peak (zero to $\pm 38.4 \times 10^{-3}$ m_0c). For each spectra, a total of 2.0×10^6 counts were accumulated in order to reduce the statistical error.

3. Results and discussion

The SRIM result shows that the maximum irradiation depths of helium implantation and vacancy production are about 310 nm and 300 nm, and the peaks of helium atoms and vacancies are located at about 200 nm and 150 nm, respectively. The displacement damage (vacancies produced/atom = displacement per atom or dpa) and the vacancy distribution have the following relationship [13]:

$$V\left[\text{vacancies (ions nm)}^{-1}\right] \times \left(\frac{10^7\,[\text{nm cm}^{-1}] \times \text{Fluence [ions cm}^{-2}]}{D_{\text{atoms}}\,[\text{atoms cm}^{-3}]}\right) = \text{dpa}, \quad (1)$$

where V is the value of the vacancy distribution [0.5488 vacancies (ions nm)$^{-1}$]. D_{atoms} is the atomic density of the material (the value of D_{atoms} for nickel is 9.127×10^{22} atoms cm^{-3}). The helium irradi-

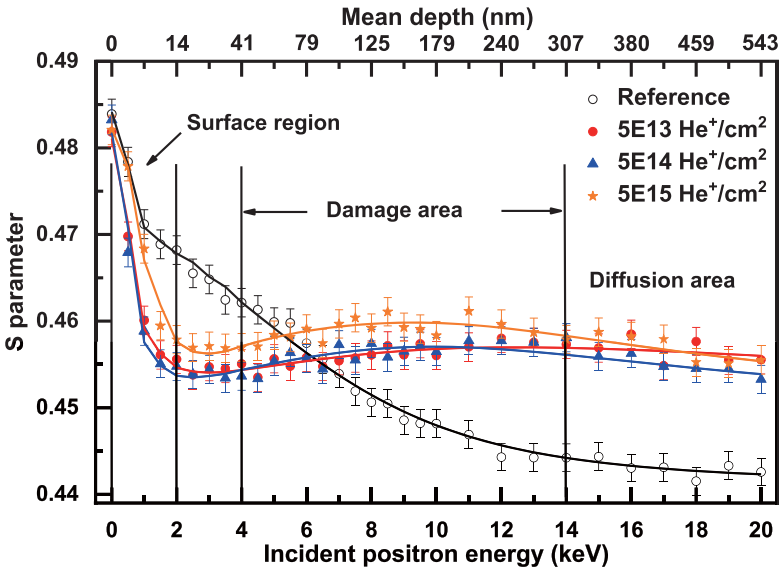

Fig. 2 S parameter as a function of incident positron energy (mean implantation depth) for nickel. The data points of S parameter are fitted by VEPFIT program.

ation fluences are 5×10^{13} He^+ cm^{-2}, 5×10^{14} He^+ cm^{-2}, and 5×10^{15} He^+ cm^{-2} in the present work. According to the Eq. (1), the irradiation damages are 0.003 dpa, 0.03 dpa and 0.3 dpa, respectively. In addition, the ratio (m/n) of vacancy to helium atoms has a high value in the surface region (zero to 14 nm), and decreases slowly with increasing target depth. The mean ratio of vacancy to helium atoms is 131. Actually, the SRIM simulation uses a temperature of 0 K ignoring thermal effects [14]. The experimental value of the ratio (m/n) is therefore expected to be lower than the calculated value shown in Fig. 1.

DBS was used to characterize the defect distribution after helium irradiation, in order to investigate the effect of helium irradiation fluence on the helium irradiation-induced defect distribution. The DBS results are shown in Fig. 2. The top X-axis of Fig. 2 is the mean positron penetration depth. The depth was estimated by the following experimental equation [15]:

$$Z(E) = \frac{40000}{\rho}E^{1.6}, \tag{2}$$

where Z is the mean positron penetration depth in units of nm, E is the incident positron energy in units of keV, and ρ is the density of material in units of $kg\,m^{-3}$ (in the present work, the density of nickel is 8.895×10^3 $kg\,m^{-3}$).

Figure 2 shows the variation of the S parameter as a function of incident positron energy. It is noticed that the S parameter of a reference specimen is largest in the surface region because of the surface effect, including positron backscattering and production of positronium [16]. The S parameter of the reference specimen then decreases slowly. After helium irradiation, many vacancy type defects are generated in the surface region according to the SRIM result. It means that the positrons are easily trapped at vacancies and annihilate with electrons around the open space defects (vacancy) in the irradiated specimens. Therefore, the positron diffusion length of irradiated specimens was shorter than that of the reference specimen. It could also illustrate the existence of open space defects (vacancy) which could weaken the influence of the surface effect. Hence, the S parameter of the irradiated specimens decreases rapidly at surface area. Whereafter, the S parameter increased at the damage area (41 nm–307 nm) because this is the main generating area of vacancy by helium ion irradiation. The density of vacancies is higher in the damage area compared with the other areas (surface area

and diffusion area) according to the SRIM result. The positron trapping rate k is proportional to the vacancy density C_v [17]:

$$k = \mu C_v, \tag{3}$$

where μ is the defect trapping coefficient. There is a positive correlation between the positron trapping rate k and the vacancy density C_v. Vacancies are easily aggregated and form vacancy clusters, and the value of the positron trapping rate k has a positive correlation with the size of the vacancy cluster [18, 19]. It is known that vacancies and vacancy clusters are helium atom trapping states, which can form He_nV_m clusters. The stability of He_nV_m clusters is related to their structure and the vacancy-to-He ratio. The He_nV_m clusters always have highly symmetric structures corresponding to their minimum energy configurations of He_nV_m clusters. The clusters have lowest energy configuration when the ratio of vacancy-to-He of He_nV_m clusters is 1 : 1 [20]. He_nV_m clusters can generate vacancy-interstitial pairs when the ratio of vacancy-to-He is less than 1 and can absorb helium atoms when the ratio of vacancy-to-He is more than 1. According to the SRIM result, the mean ratio of vacancy to helium atoms is 131 which is significantly more than 1. Therefore, the He_nV_m clusters also belong to open space defects, and the characteristics of positron trapping at these clusters are similar to vacancy clusters. In the conventional positron trapping model, the total number of positrons annihilating in defects (N_d) has the following relationship with positron trapping rate k [17]:

$$N_d = \frac{1}{1 + \lambda_f/k} \cdot N_0, \tag{4}$$

where N_0 is the total number of incident positrons and λ_f is the positron annihilation rate in the perfect lattice. The S parameter can be divided into two parts, S_f and S_d corresponding to the value of S when all positrons annihilate in the crystal lattice or in defect states, respectively. Therefore, the S parameter can be written as [21]:

$$S = \frac{S_f \cdot (N_0 - N_d) + S_d \cdot N_d}{N_0} \tag{5}$$

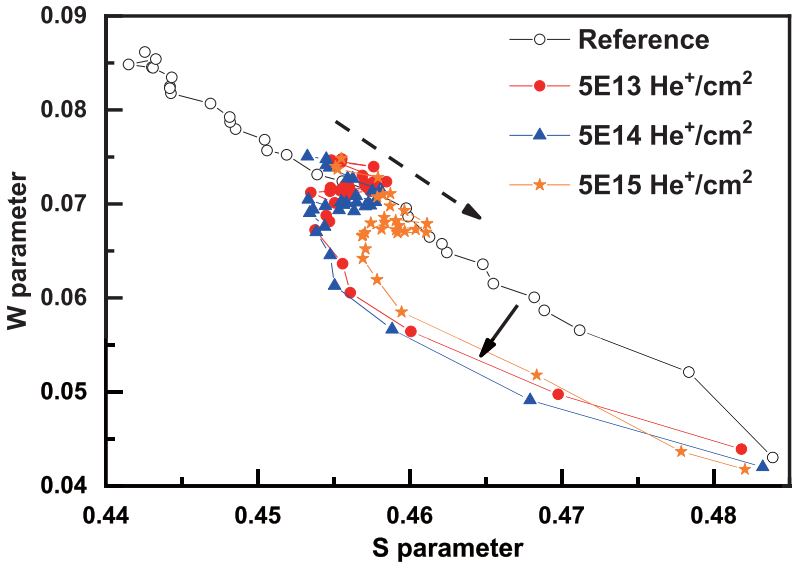

Fig. 3 S–W plot for a non-irradiated reference nickel specimen, together with plots for the specimens irradiated with different helium irradiation fluence.

According to Eq. (3), Eq. (4) and Eq. (5), it could illustrate that the S parameter has a positive correlation with positron trapping rate k. In the damage area, the density and size of open space defect clusters (He_nV_m clusters) increases with increasing helium irradiation fluence [22]. The positron trapping rate k and the number of positrons annihilated around defects increase with increasing defect density and the size of open space defects (He_nV_m clusters). Therefore, the S parameter also has a positive correlation with the density and sizes of defects. The migration energy of vacancies and helium atoms in nickel are 1.17 eV and 0.078 eV, respectively. Hence, helium atoms can migrate deeper than vacancies. The helium atoms tend to agglomerate with each other and form helium atom clusters, and such clusters could induce a vacancy and self-interstitial when the number of helium atoms exceeds 5 [20, 23, 24]. In the diffusion area, the density of open space defects was lower than that of the damage area. Therefore, the S parameter keeps decreasing in the diffusion area.

Further information about the positron annihilation mechanism with different types of defects can be obtained by plotting the S and W parameters against each other, the so-called S–W plot [25]. S–W plots for a non-irradiated reference nickel specimen, together with the 3 specimens irradiated with different helium irradiation fluence are shown in Fig. 3. The S–W curve of the reference specimen shows a linear relationship suggesting that the positron annihilation mechanism is similar at each annihilation site. After helium irradiation, the S–W plots deviate from the reference plot and show a linear relationship (solid arrow) in the surface region because most positrons are trapped by vacancy type defects and annihilate with electrons around this defect. In the damage area, the linear relationship fades away and the data points tend to aggregate together. The gathering of data points along the direction of the dashed arrow suggests that the positron annihilation mechanism is similar in each of these irradiated specimens. After helium irradiation, many vacancies were introduced in the specimen, and He_nV_m clusters were formed due to combination between vacancies and helium atoms. In the helium irradiation process, higher fluence needs a longer irradiation time for the same flux. Therefore, the helium atoms and vacancies have more time to diffuse, nucleate and grow, resulting in larger sized He_nV_m clusters [22]. The size of open spaces increases with increasing size of He_nV_m clusters when the ratio (m/n) is constant. The positron trapping rate and the number of positrons annihilated around He_nV_m clusters are increased with increasing He_nV_m clusters size. Therefore, the S–W plots indicate the relative change of the size of He_nV_m clusters, suggesting that their size increased with increasing helium irradiation fluence (dashed arrow).

4. Conclusion

Helium irradiation was carried out using 50 keV He^{2+} ions in nickel at room temperature, and irradiation fluences were 5×10^{13} $He^+\,cm^{-2}$, 5×10^{14} $He^+\,cm^{-2}$, and 5×10^{15} $He^+\,cm^{-2}$. DBS was used to investigate the effect of helium irradiation fluence on He_nV_m clusters evolution. After helium irradiation, the existence of open space defects seems to weaken the influence of the surface effect. In the damage area, the helium atoms combined with vacancies to form He_nV_m clusters and the size of He_nV_m clusters increased with increasing helium irradiation fluence.

Acknowledgment

This work is supported by the National Science Foundation of China 11475193, 11505192 and 11575205.

References

[1] L. Mathieu, D. Heuer, E. Merle-Lucotte, R. Brissot, C. Le Brun, E. Liatard, J. M. Loiseaux, O. Méplan, and A. Nuttin, Nucl. Sci. Eng. **161**, 78 (2009).
[2] L. Mathieu, D. Heuer, R. Brissot, C. Garzenne, C. Le Brun, D. Lecarpentier, E. Liatard, J. M. Loiseaux, O. Méplan, E. Merle-Lucotte, A. Nuttin, E. Walle, and J. Wilson, Prog. Nucl. Energy **48**, 664 (2006).
[3] C.-W. Sun, R. Hui, W. Qu, and S. Yick, Corrosion Sci. **51**, 2508 (2009).

[4] M. D. Bermejo, and M. J. Cocero, AICHE J. **52**, 3933 (2006).
[5] S. Saini, R. Menon, S. K. Sharma, A. P. Srivastava, S. Mukherjee, P. Y. Nabhiraj, P. K. Pujari, D. Srivastava, and G. K. Dey, J. Nucl. Mater. **479**, 279 (2016).
[6] E. E. Bloom, J. Nucl. Mater. **258**, 7 (1998).
[7] J. Chen, Z. Y. He, and P. Jung, Acta Mater. **54**, 1607 (2006).
[8] R. Vassen, H. Trinkaus, and P. Jung, Phys. Rev. B. **44**, 4206 (1991).
[9] D. Kramer, H. R. Brager, C. G. Rhodes, and A. G. Pard, J. Nucl. Mater. **25**, 121 (1968).
[10] H. Ohkubo, Z. Tang, Y. Nagai, M. Hasegawa, T. Tawara, and M. Kiritani, Mater. Sci. Eng. A-Struct. Mater. Prop. Microstruct. Process. **350**, 95 (2003).
[11] C. D. Hardie, C. A. Williams, S. Xu, and S. G. Roberts, J. Nucl. Mater. **439**, 33 (2013).
[12] G. E. Lee-Whiting, Phys. Rev. **97**, 1557 (1955).
[13] G. W. Egeland, J. A. Valdez, S. A. Maloy, K. J. McClellan, K. E. Sickafus, and G. M. Bond, J. Nucl. Mater. **435**, 77 (2013).
[14] J. F. Ziegler, Nucl. Instrum. Methods **168**, 17 (1980).
[15] J. Qiu, Y. Xin, X. Ju, L. P. Guo, B. Y. Wang, Y. R. Zhong, Q. Y. Huang, and Y. C. Wu, Nucl. Instrum. Methods Phys. Res. Sect. B-Beam Interact. Mater. Atoms **267**, 3162 (2009).
[16] H. Huomo, A. Vehanen, M. D. Bentzon, and P. Hautojarvi, Phys. Rev. B **35**, 8252 (1987).
[17] M. Abdelrahman, Jpn. J. Appl. Phys **36**, 6530 (1997).
[18] C. H. Hodges, Phys. Rev. Lett. **25**, 284 (1970).
[19] R. M. Nieminen and J. Laakkonen, Appl. Phys. **20**, 181 (1979).
[20] H. F. Gong, C. B. Wang, W. Zhang, J. Xu, P. Huai, H. Q. Deng, and W. Y. Hu, Nucl. Instrum. Methods Phys. Res. Sect. B-Beam Interact. Mater. Atoms **368**, 75 (2016).
[21] J. Baram and M. Rosen, Phys. Status Solidi A-Appl. Mat. **16**, 263 (1973).
[22] X. L. Zhou, H. F. Huang, R. Xie, G. J. Thorogood, C. Yang, Z. J. Li, and H. J. Xu, J. Nucl. Mater. **467**, 848 (2015).
[23] W. D. Wilson, C. L. Bisson, and M. I. Baskes, Phys. Rev. B. **24**, 5616 (1981).
[24] M. I. Baskes and W. D. Wilson, Phys. Rev. B. **27**, 2210 (1983).
[25] X. B. Liu, R. S. Wang, J. Jiang, Y. C. Wu, C. H. Zhang, A. Ren, C. L. Xu, and W. J. Qian, J. Nucl. Mater. **451**, 249 (2014).